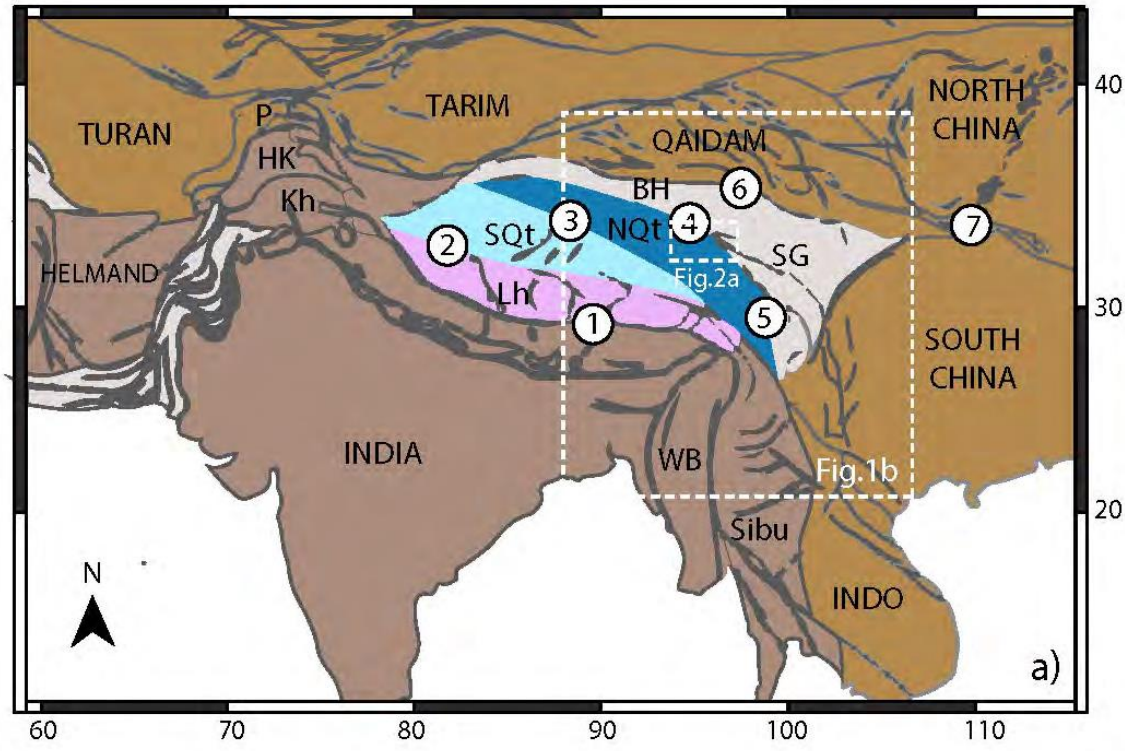
TURAN
P
HK
Kh
TARIM
QAIDAM
NORTH CHINA
BH
NQt
SQt
Lh
SG
HELMAND
Fig.2a
Fig.1b
SOUTH CHINA
INDIA
WB
Sibu
INDO
N
a)
40
30
20
60
70
80
90
100
110

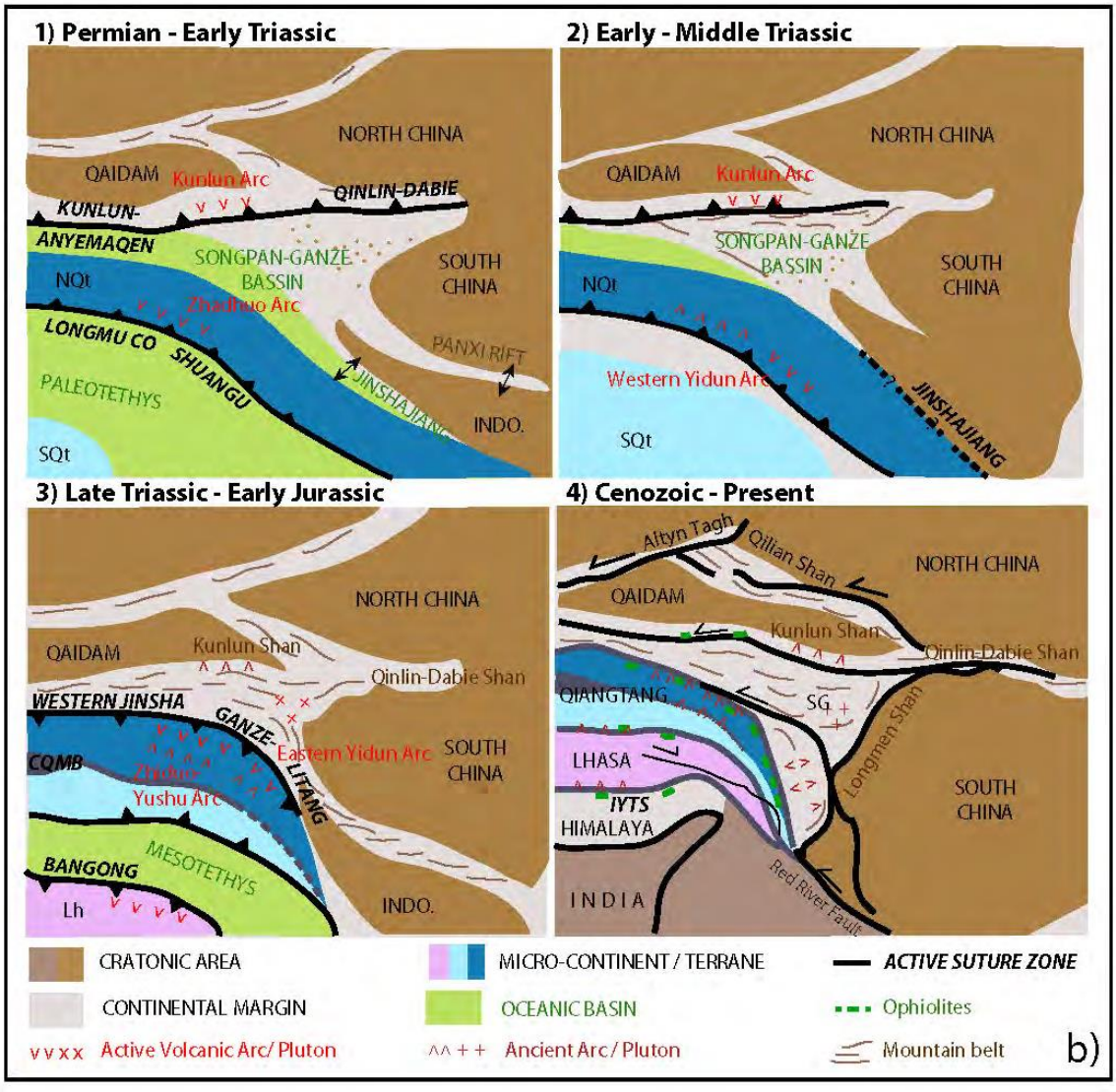
1) Permian - Early Triassic
NORTH CHINA
QAIDAM
Kunlun Arc
QINLIN-DABIE
KUNLUN-
ANYEMAQEN
SONGPAN-GANZE
BASSIN
SOUTH CHINA
NQt
Zhanhuo Arc
LONGMU CO
SHUANGU
PANXI RIFT
JINSHAJIANG
PALEOTETHYS
INDO.
SQt
2) Early - Middle Triassic
NORTH CHINA
QAIDAM
Kunlun Arc
SONGPAN-GANZE
BASSIN
SOUTH CHINA
NQt
Western Yidun Arc
JINSHAJIANG
SQt
3) Late Triassic - Early Jurassic
NORTH CHINA
QAIDAM
Kunlun Shan
Qinlin-Dabie Shan
WESTERN JINSHA
GANZE-
LITANG
Eastern Yidun Arc
SOUTH CHINA
CQMB
Zhidoi-
Yushu Arc
MESOTETHYS
BANGONG
Lh
INDO.
4) Cenozoic - Present
Altyn Tagh
Qilian Shan
NORTH CHINA
QAIDAM
Kunlun Shan
Qinlin-Dabie Shan
QIANGTANG
SG
Longmen Shan
LHASA
IYTS
HIMALAYA
SOUTH CHINA
INDIA
Red River Fault
CRATONIC AREA
MICRO-CONTINENT / TERRANE
ACTIVE SUTURE ZONE
CONTINENTAL MARGIN
OCEANIC BASIN
Ophiolites
v v x x Active Volcanic Arc/ Pluton
^^ + + Ancient Arc / Pluton
Mountain belt
b)

Figure 1. a) General map of Southern Asia showing the main continental terranes and the associated suture zones discussed in text (1-10). Two inserts indicate the locations of Figures 1b and 2a. Suture zones: 1, Indus-Yarlung-Zangbo; 2, Bangong Nujiang; 3, Longmu Co-Shanghu; 4, Western Jinsha; 5, Ganze-Litang; 6, Kunlun–Anyemaqen Suture; 7, Qinlin-Dabie. **b)** Summary of the Paleozoic-Mesozoic episodes of Tibetan continental accretion. Modified from Roger et al. (2010) and Yang et al. (2014). Abbreviations: BH, Bayan Har; CQMB, Central Qiangtang Metamorphic Belt; HK, Hindu Kush; INDO, Indochina; Kh, Kohistan; Lh, Lhasa; NQt, North Qiangtang; P, Pamir; SG, Songpan-Ganze; Sibu, Sibumasu; SQt, South Qiangtang; WB, West Burma.

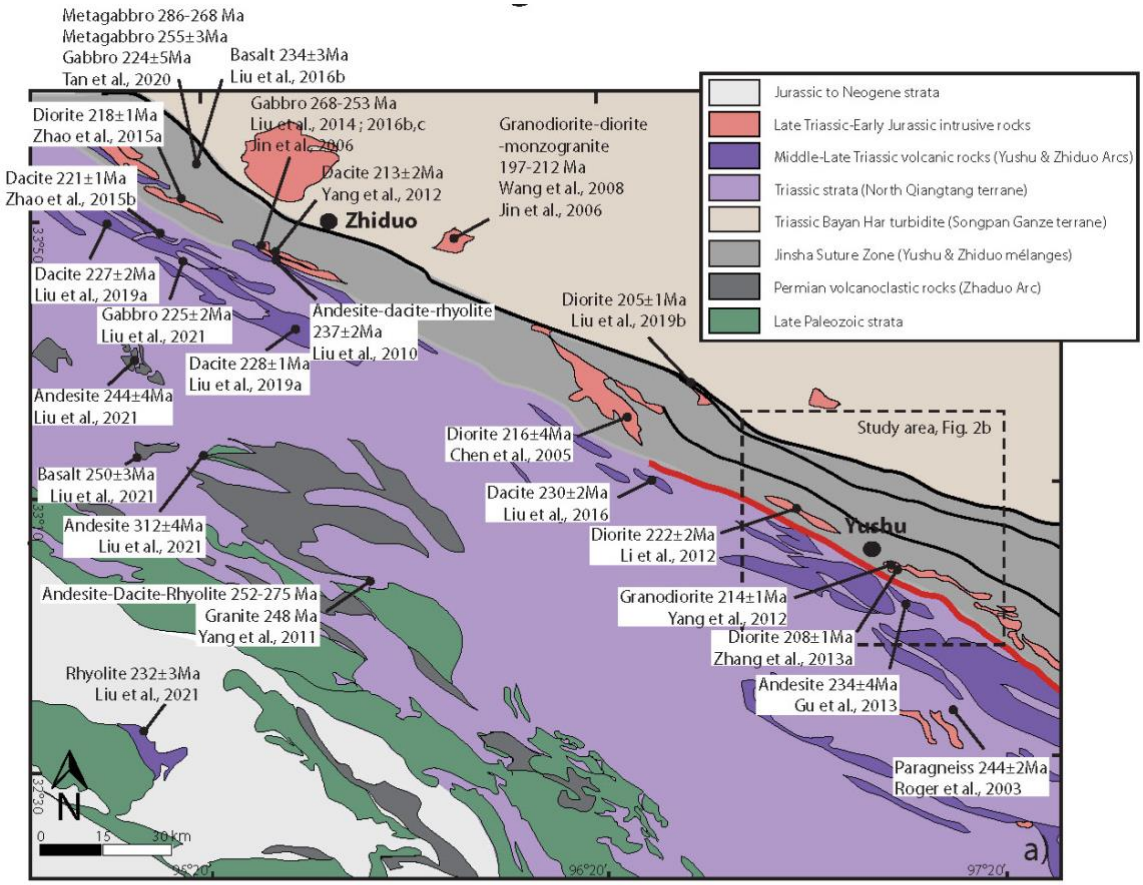
Metagabbro 286-268 Ma
Metagabbro 255±3Ma
Gabbro 224±5Ma
Tan et al., 2020
Basalt 234±3Ma
Liu et al., 2016b
Diorite 218±1Ma
Zhao et al., 2015a
Gabbro 268-253 Ma
Liu et al., 2014 ; 2016b,c
Jin et al., 2006
Granodiorite-diorite
-monzogranite
197-212 Ma
Wang et al., 2008
Jin et al., 2006
Dacite 221±1Ma
Zhao et al., 2015b
Dacite 213±2Ma
Yang et al., 2012
Zhiduo
Dacite 227±2Ma
Liu et al., 2019a
Gabbro 225±2Ma
Liu et al., 2021
Andesite-dacite-rhyolite
237±2Ma
Liu et al., 2010
Diorite 205±1Ma
Liu et al., 2019b
Dacite 228±1Ma
Liu et al., 2019a
Andesite 244±4Ma
Liu et al., 2021
Diorite 216±4Ma
Chen et al., 2005
Study area, Fig. 2b
Basalt 250±3Ma
Liu et al., 2021
Dacite 230±2Ma
Liu et al., 2016
Andesite 312±4Ma
Liu et al., 2021
Diorite 222±2Ma
Li et al., 2012
Yushu
Andesite-Dacite-Rhyolite 252-275 Ma
Granite 248 Ma
Yang et al., 2011
Granodiorite 214±1Ma
Yang et al., 2012
Diorite 208±1Ma
Zhang et al., 2013a
Rhyolite 232±3Ma
Liu et al., 2021
Andesite 234±4Ma
Gu et al., 2013
Paragneiss 244±2Ma
Roger et al., 2003
Jurassic to Neogene strata
Late Triassic-Early Jurassic intrusive rocks
Middle-Late Triassic volcanic rocks (Yushu & Zhiduo Arcs)
Triassic strata (North Qiangtang terrane)
Triassic Bayan Har turbidite (Songpan Ganze terrane)
Jinsha Suture Zone (Yushu & Zhiduo mélanges)
Permian volcanoclastic rocks (Zhaduo Arc)
Late Paleozoic strata
N
0 15 30 km
96°20'
97°20'
a)

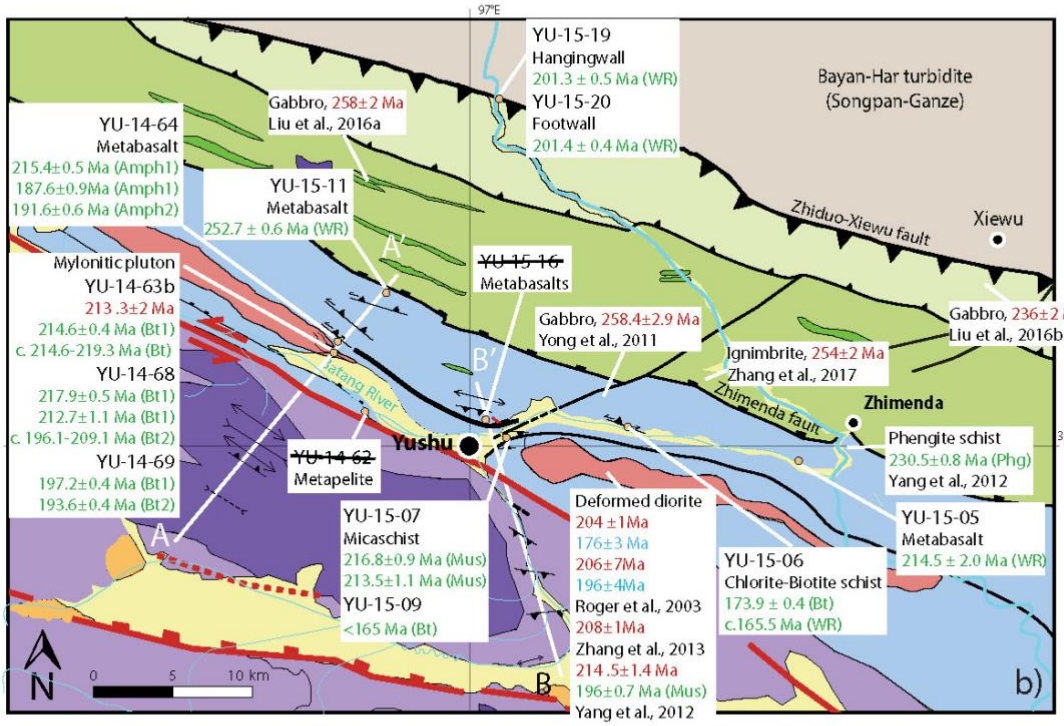
97°E
YU-15-19
Hangingwall
201.3 ± 0.5 Ma (WR)
YU-15-20
Footwall
201.4 ± 0.4 Ma (WR)
Bayan-Har turbidite
(Songpan-Ganze)
Gabbro, 258±2 Ma
Liu et al., 2016a
YU-14-64
Metabasalt
215.4±0.5 Ma (Amph1)
187.6±0.9Ma (Amph1)
191.6±0.6 Ma (Amph2)
YU-15-11
Metabasalt
252.7 ± 0.6 Ma (WR)
Zhiduo-Xiewu fault
Xiewu
A'
YU-15-16
Metabasalts
Mylonitic pluton
YU-14-63b
213 .3±2 Ma
214.6±0.4 Ma (Bt1)
c. 214.6-219.3 Ma (Bt)
Gabbro, 258.4±2.9 Ma
Yong et al., 2011
Gabbro, 236±2 Ma
Liu et al., 2016b
Ignimbrite, 254±2 Ma
Zhang et al., 2017
B'
Jatang River
Zhimenda fault
Zhimenda
YU-14-68
217.9±0.5 Ma (Bt1)
212.7±1.1 Ma (Bt1)
c. 196.1-209.1 Ma (Bt2)
YU-14-69
197.2±0.4 Ma (Bt1)
193.6±0.4 Ma (Bt2)
Yushu
YU-14-62
Metapelite
Phengite schist
230.5±0.8 Ma (Phg)
Yang et al., 2012
33°N
Deformed diorite
204 ±1Ma
176±3 Ma
206±7Ma
196±4Ma
Roger et al., 2003
208±1Ma
Zhang et al., 2013
214 .5±1.4 Ma
196±0.7 Ma (Mus)
Yang et al., 2012
YU-15-07
Micaschist
216.8±0.9 Ma (Mus)
213.5±1.1 Ma (Mus)
YU-15-09
<165 Ma (Bt)
YU-15-06
Chlorite-Biotite schist
173.9 ± 0.4 (Bt)
c.165.5 Ma (WR)
YU-15-05
Metabasalt
214.5 ± 2.0 Ma (WR)
A
B
N
0 5 10 km
b)
Songpang-Ganze terrane
Bayan Har Triassic flysch
Qiangtang terrane
Quaternary deposits
Cenozoic strata
Upper Triassic strata
Upper Triassic Yushu Arc volcanics/plutons
Yushu mélange
Upper stratigraphic units
- conglomerate, sandstone, limestone, dark grey slate, chlorite schist + ultramafic rocks
Lower «Tectonostratigraphic» unit
- blueschist to greenschist facies alternations of metabasalt, marble, phyllite, metagreywacke
Ultramafic lenses
Fold axis trace
Left-lateral fault
Inferred fault
Thrust
Normal fault
River
Active Yushu Fault (after Chevalier et al., 2018)
Dating methods:
204 ±1Ma U-Pb on zircon
176±3 Ma Rb-Sr on feldspar and/or whole-rock
Ar-Ar on (mineral)
217.9±0.5 Ma (Bt1) Plateau age
212.7±1.1 Ma (Bt1) Pseudo-plateau age
c. 196.1-209.1 Ma (Bt2) Apparent ages
Sampling sites

Figure 2. a) Geological map of the Yushu-Zhiduo area in northeastern Qiangtang, showing the distribution of recently dated Mesozoic magmatic rocks along the Western Jinsha Suture. Modified from Liu et al. (2021) and Yang et al. (2014). The location of our study area is indicated by the insert. **b)** Map of the Yushu mélange and adjacent areas, modified from Yang et al. (2012), Zhang et al. (2017) and the Geological Survey of Qinghai Province 1:250 000 Geological Map (2005), according to our observations. Available age data for magmatic and deformed rocks are reported. AA' and BB' indicate respectively the western and eastern cross-sections of Figure 3a,b.

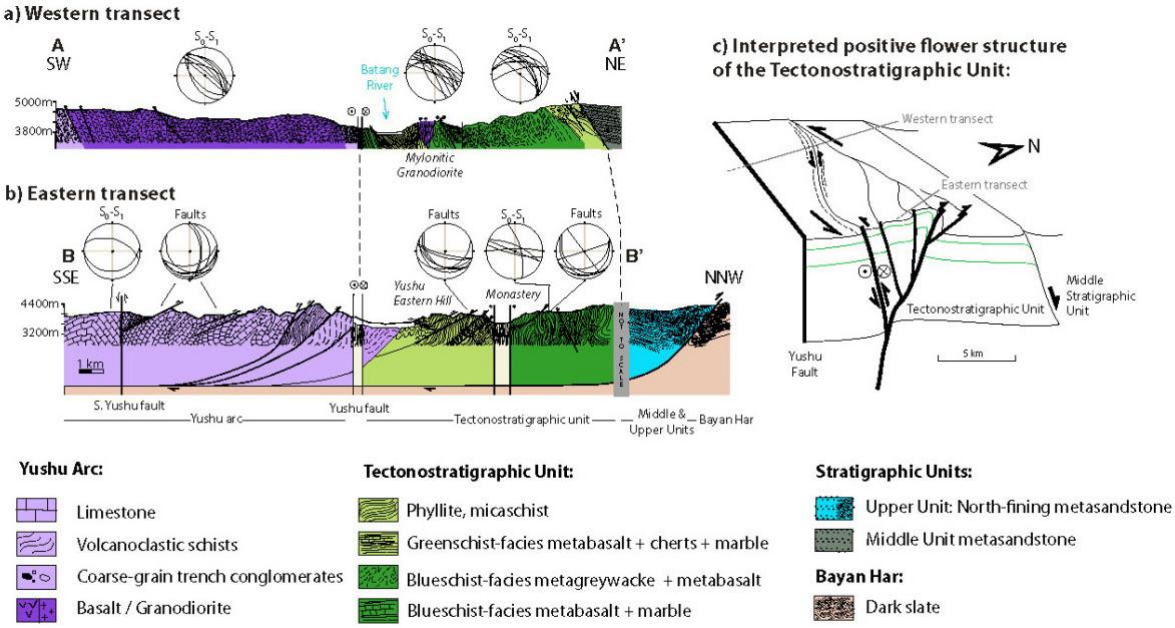

Figure 3. a-b) Structural cross-sections of the Yushu mélange, with stereographic projections (lower hemisphere, equal area net) of the observed fabrics. **c)** Schematic interpretation of the structures of the *Tectonostratigraphic* unit as part of a large-scale positive flower structure, resulting from regional transpressive deformation (see the text for explanation).

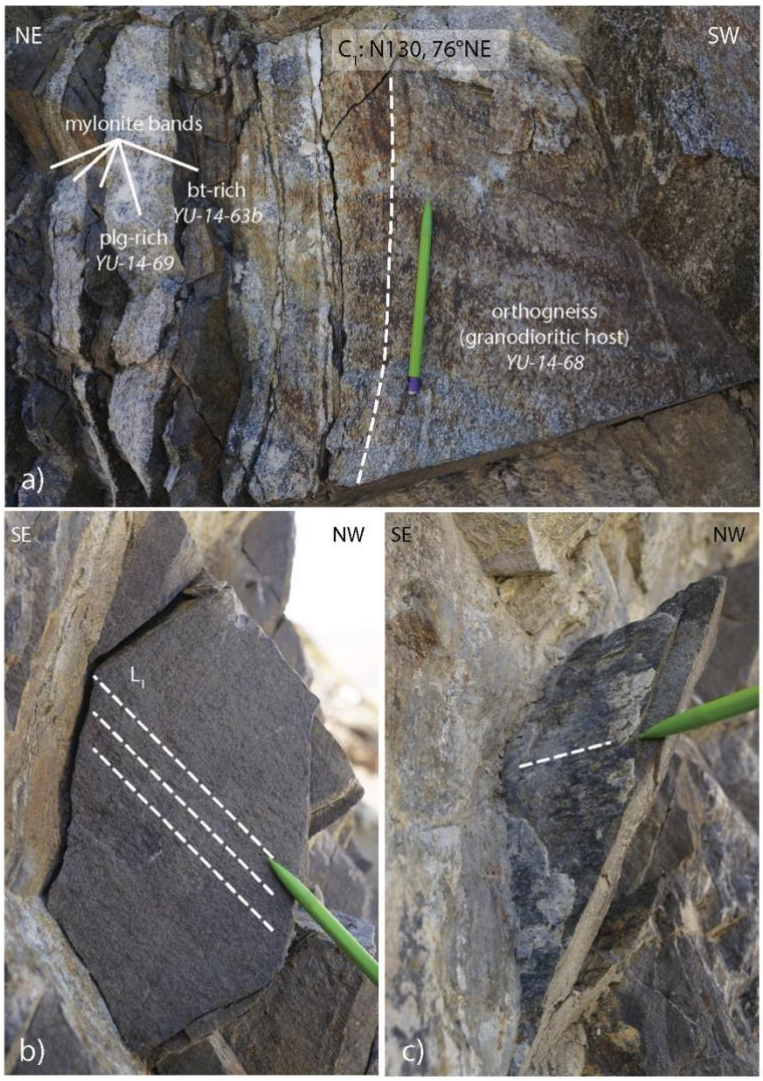

Figure 4. Outcrop pictures of the mylonitic granodiorite pluton (western transect). **a)** Heterogeneous composition of the pluton, with mylonite bands wrapping a much less deformed granodiorite lens. The main C_1 shear planes direction is indicated. **b)** Surface of a C_1 plane within a mylonitic band, showing L_1 lineation defined by the alignment of tiny biotite flakes. **c)** Late sub-horizontal brittle striation on a slickenside, corresponding to a C_1 plane, and related to the present-day activity of the Yushu fault.

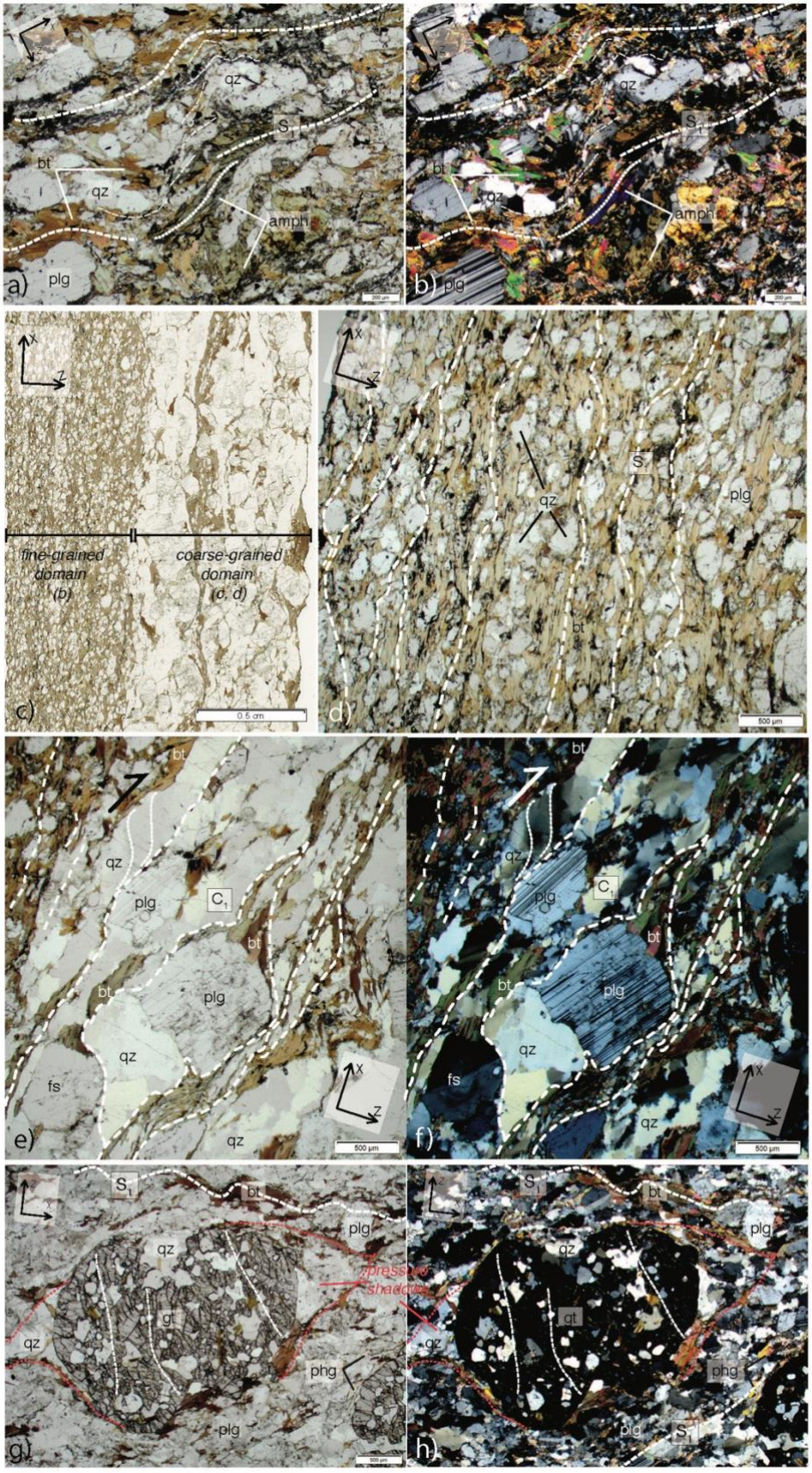

Figure 5. Interpreted optical microphotographs of samples from the mylonitic granodiorite pluton. S_1 foliation is underlined by white dashed lines; stretching direction (X)

is N130. **a-b)** Least deformed part of the granodiorite pluton (sample YU-14-68), using parallel light and crossed Nicols. **c)** Thin-section scan showing the contact between a fine-grained mylonitic band (left) and a coarse-grained orthogneiss domain (right). **d)** Fine-grained mylonitic band (sample YU-14-63b), using parallel light. **e-f)** Coarse-grained domain, using parallel light and crossed Nicols; the internal deformation of quartz grains is underlined. **g-h)** Garnet-bearing, quartz-rich mylonite band (sample YU-14-69), using parallel light and crossed Nicols; red dotted lines delineate pressure shadows. Mineral abbreviations: amph, amphibole; bt, biotite; fs, alkali feldspar; gt, garnet; plg, plagioclase; qz, quartz.

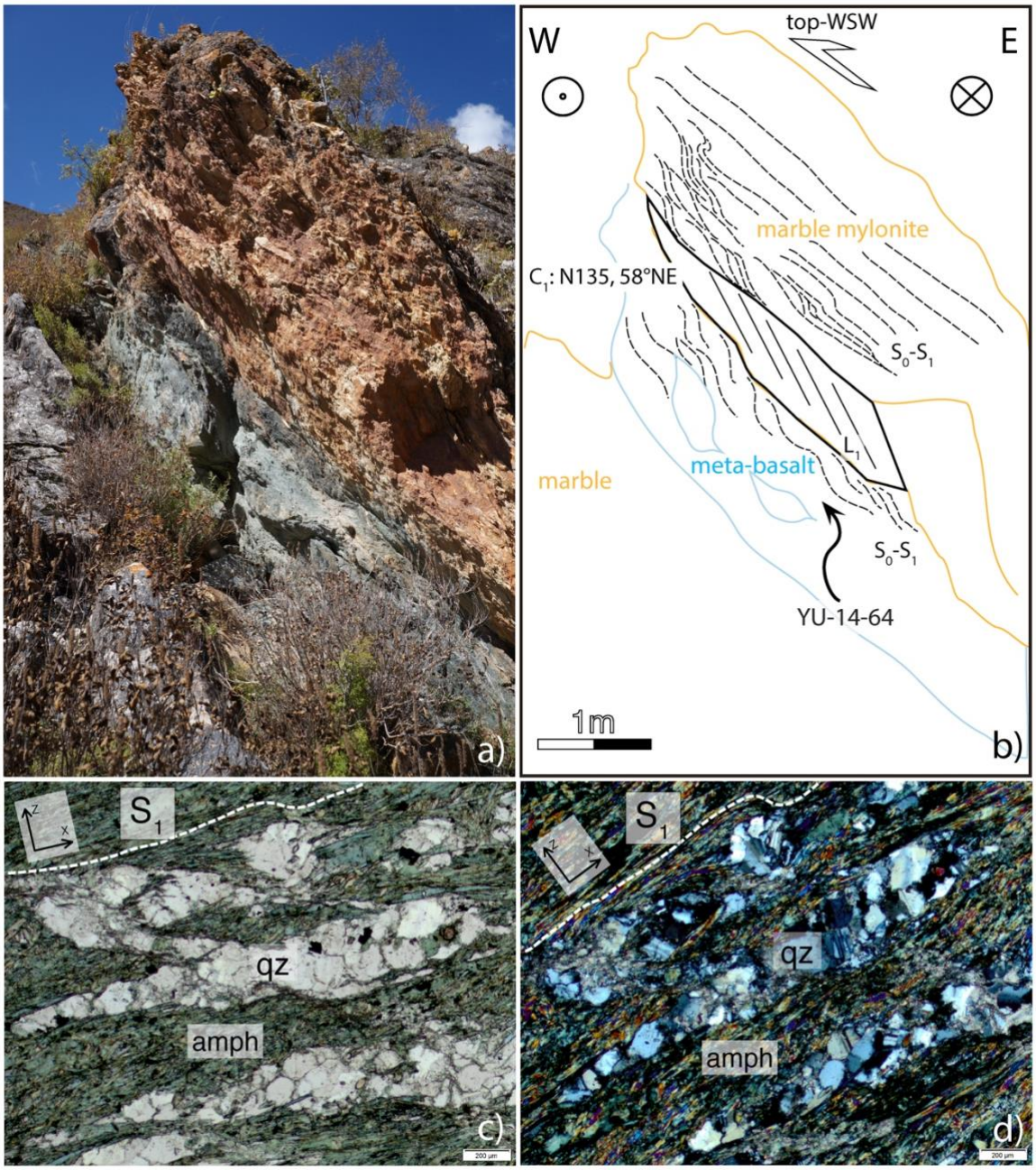

Figure 6. a) Field picture and **b)** structural interpretation of a top-to-the-WSW transpressive shear contact between marble and blueschists with metabasalt lenses (sampling site of YU-14-64). **c-d)** Interpreted microphotographs of the metabasaltic sample YU-14-64 using parallel light (c) and crossed Nicols (d). The main foliation plane S_1 is underlined with a white dashed line. Mineral abbreviations: amph, amphibole; qz, quartz, plg, plagioclase.

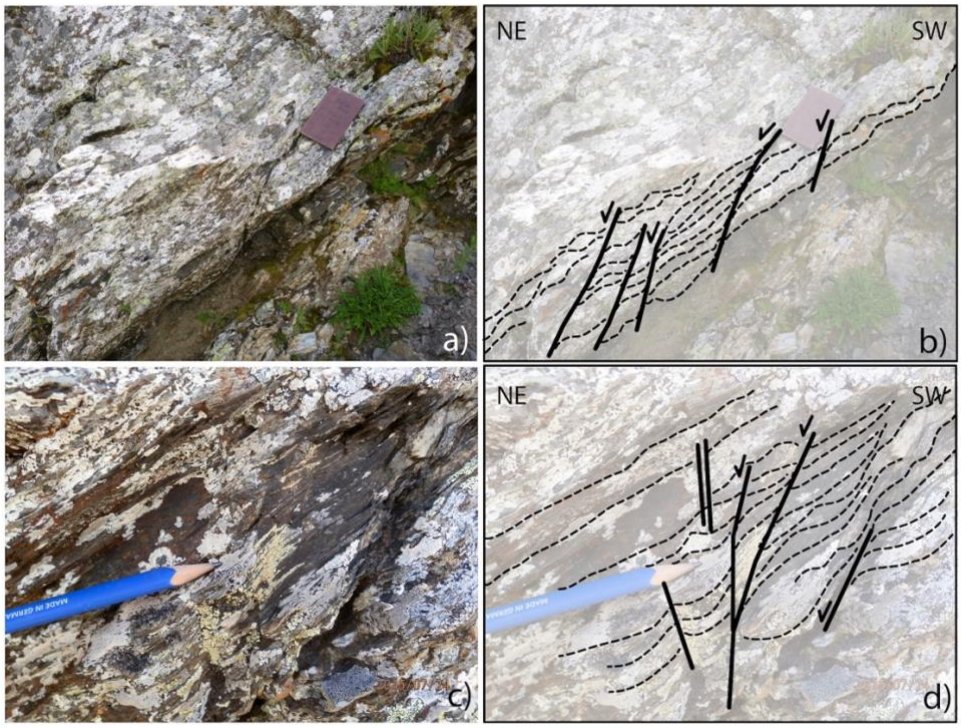

Figure 7. Field pictures (a,c) and structural interpretations (b,d) of top-to-the-NE normal shear within the hanging wall of the Zhimenda fault (sampling site of YU-15-11). Dashed lines indicate the main foliation planes, thick lines indicate shear planes.

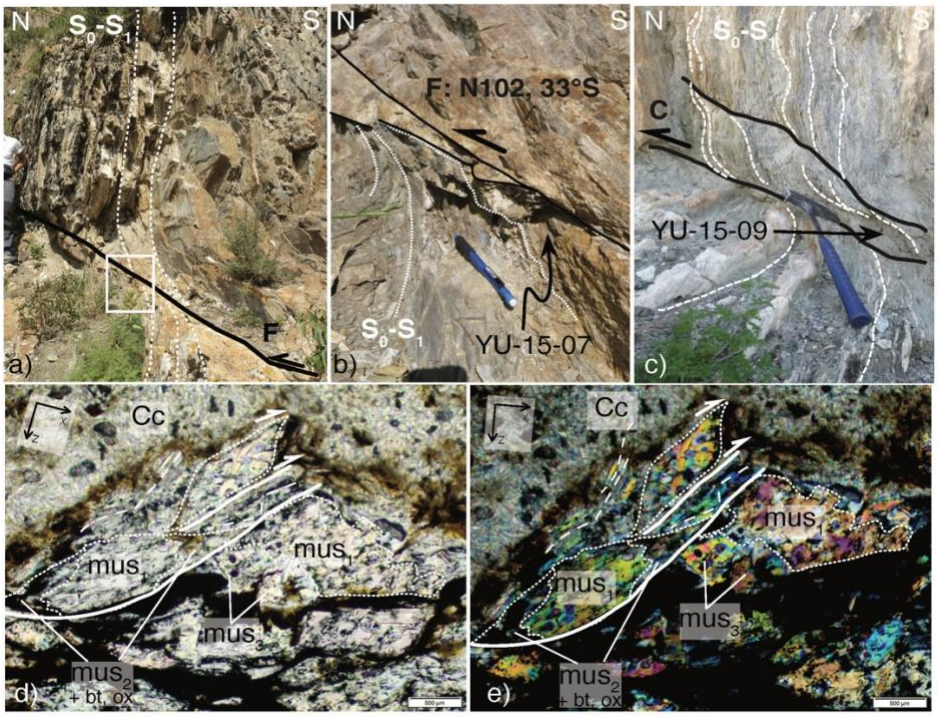

Figure 8. Top-to-the-north brittle structures affecting the subvertical S_0/S_1 schistosity on the eastern hill of the Yushu city. **a,b)** Interpreted field picture of a fault plane on muscovite-bearing schists (sampling site of YU-15-07). **c)** Interpreted field picture of a shear plane in cherts with quartz-chlorite and calcite veins (sampling site of YU-15-09). **d-e)** Interpreted microphotographs of the fault plane sample YU-14-07, using parallel light (d) and crossed Nicols (e). White dashed lines underline the foliation planes; solid white lines indicate glide planes or micro-thrusts between grains; white dotted lines delineate muscovite grain boundaries. mus_1 are deformed porphyroclasts, mus_2 and mus_3 are syn-deformation (re)crystallized grains. Mineral abbreviations: Cc, carbonate; bt, biotite; ox, oxide; mus, muscovite; qz, quartz.

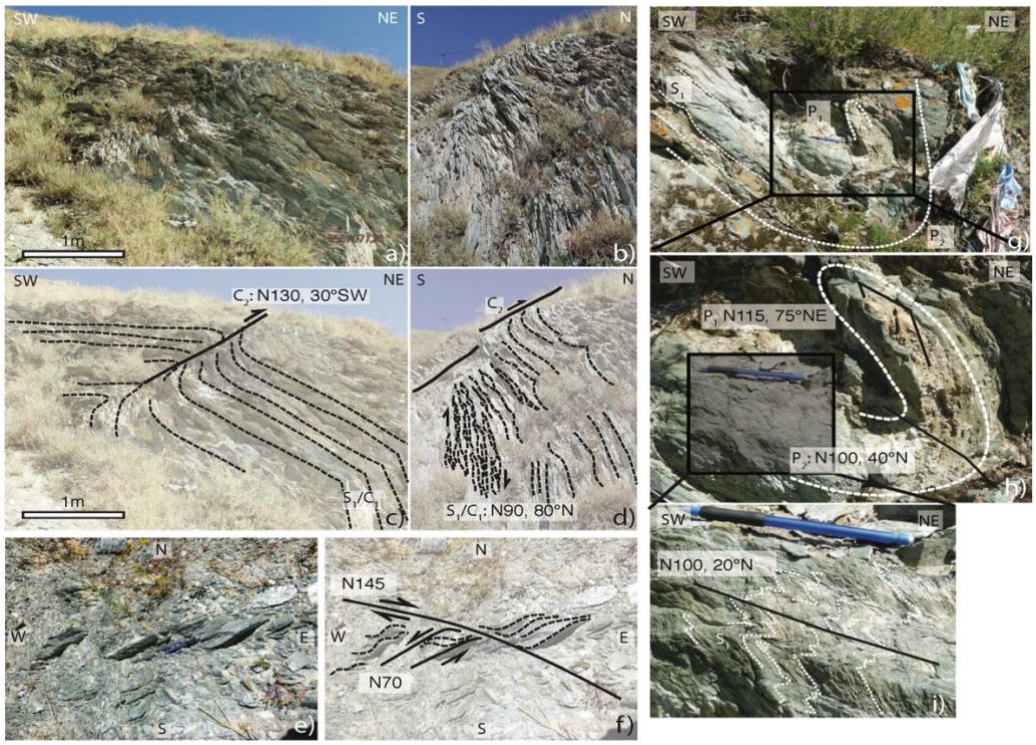

Figure 9. Ductile structures affecting blueschist-facies metabasalts on the Yushu monastery hill, north of the city (sampling sites of YU-15-16 and YU-15-17). **a,b)** Field pictures and **c,d)** structural interpretation: the main apparent subvertical foliation S_1 presents shear structures, suggesting that the foliation was transposed during a first deformation phase. This S_1/C_1 planes are affected by top-to-the-NE folding and shearing along C_2 planes. **e,f)** View from above, the subvertical S_1 foliation is affected by conjugate strike-slip vertical shear zones, indicating N-S pure-shear flattening. **g-i)** Interpreted field pictures of the two generations of folds. (h) & (i) are close-up views of the fold structure showing the orientations of P_1, P_2 and of the crenulation axial planes.

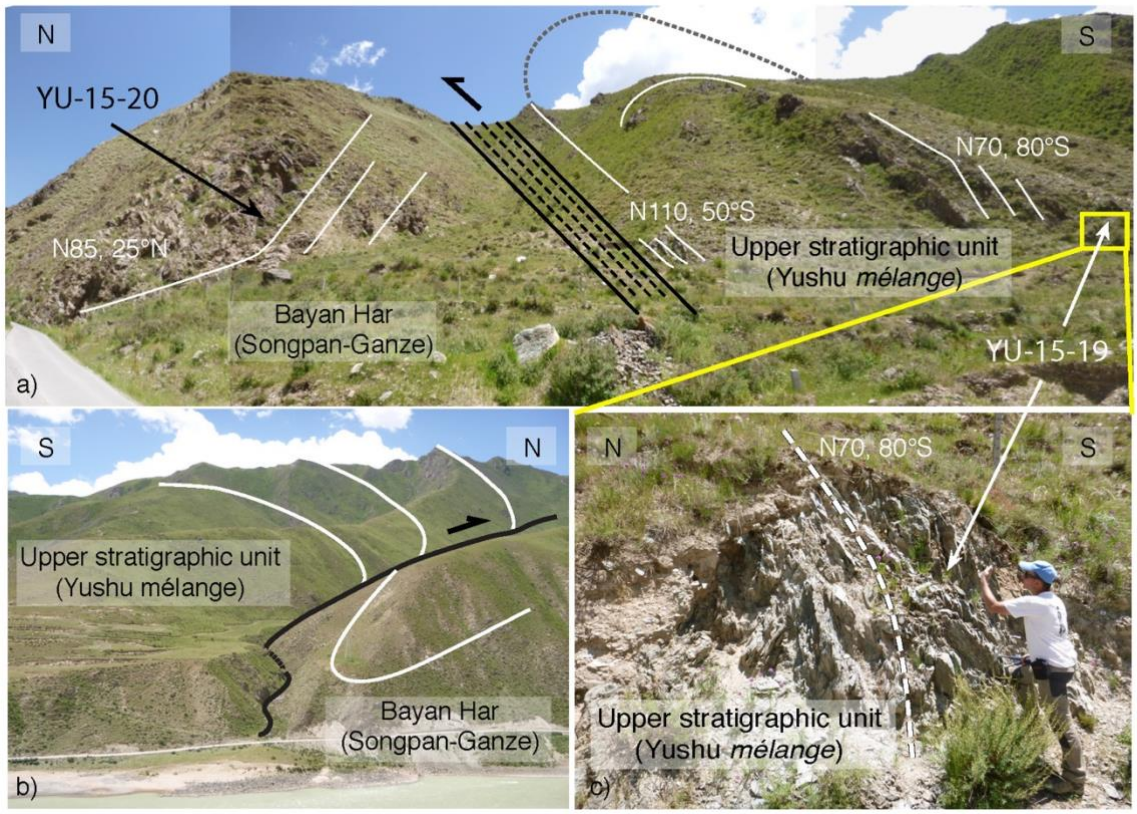

Figure 10. Top-to-the-north contact between the Yushu mélange upper stratigraphic unit and the Bayan Har turbidites of the Songpan-Ganze block, in the Zhiduo-Xiewu fault zone: **a, c)** outcrop views, with measured structural data reported (sampling site of YU-15-19 and YU-15-20); **b)** landscape view.

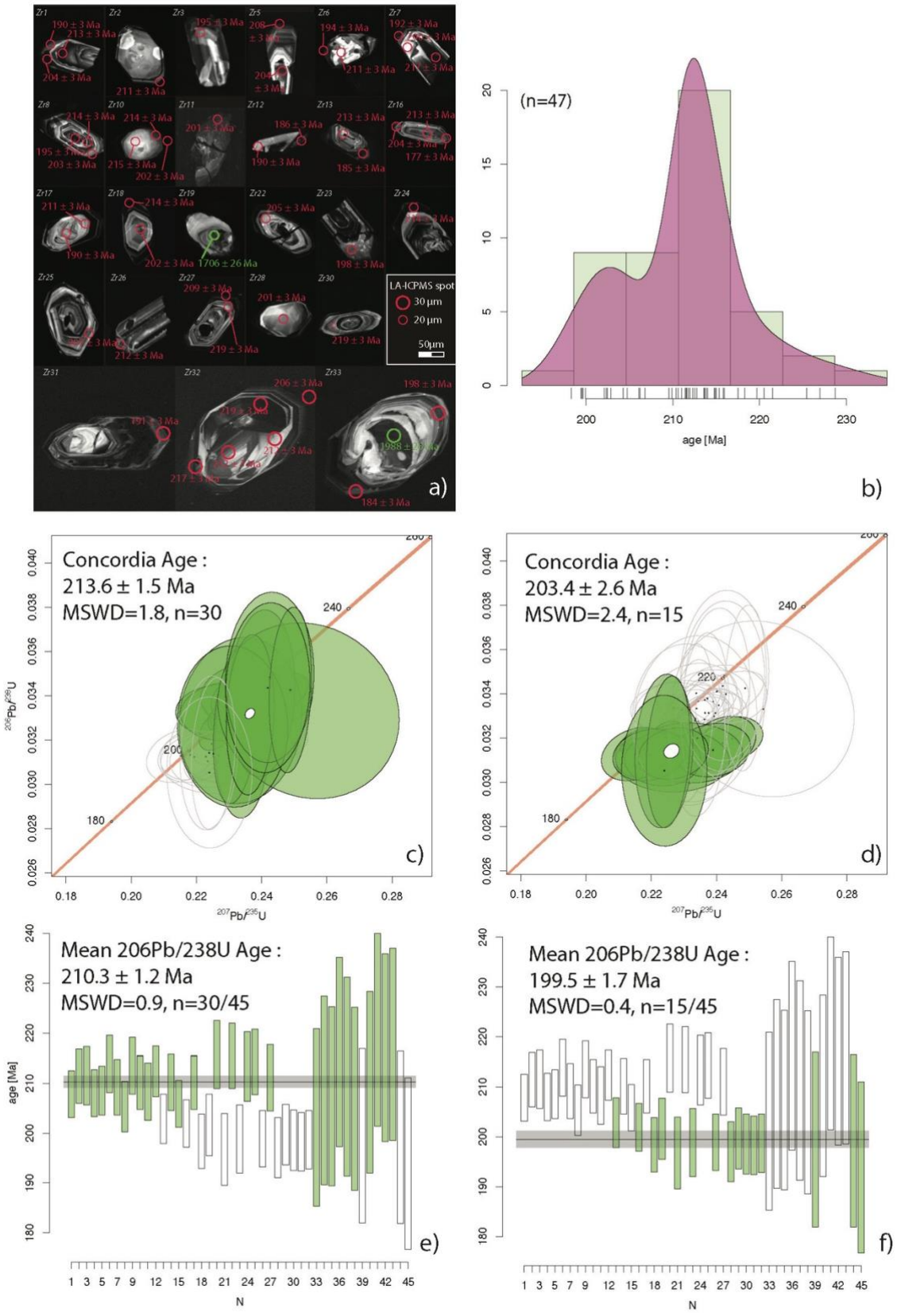

Figure 11. Zircon LA-ICP-MS U-Pb isotopic data and results for the mylonitic

granodiorite sample YU-14-63b. **a)** Zircons morphologies in CL microscopy, with laser-ablation spot locations. **b)** Zircon U-Pb age probability plots. **c,d)** Tera-Wasserburg concordia diagrams and **e,f)** mean $^{206}Pb/^{238}U$ age plots; the left panel (c,e) corresponds to the 30 oldest analyses, the right panel (d,f) to the 15 youngest.

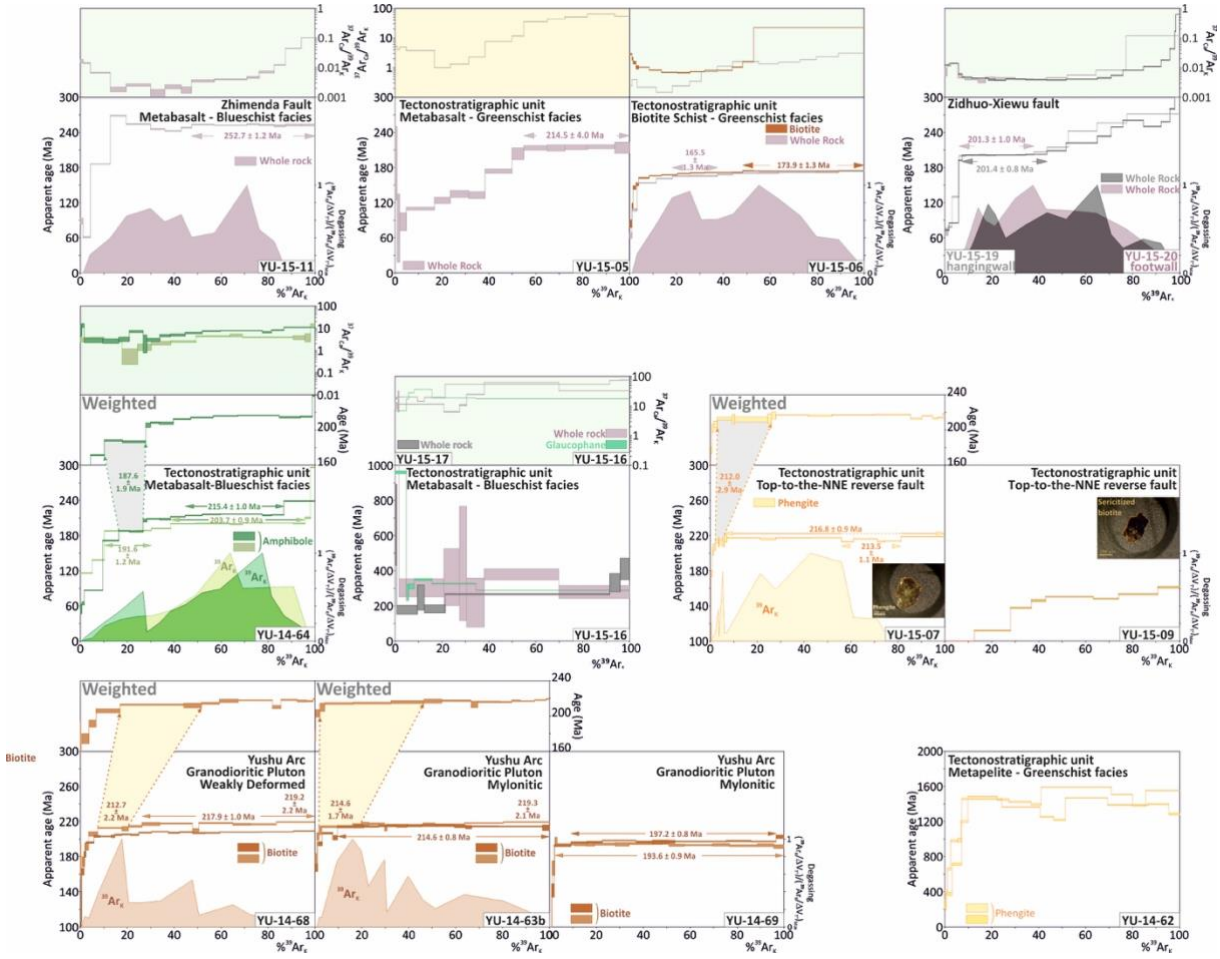

Figure 12. $^{40}Ar/^{39}Ar$ apparent age spectra of minerals and/or whole-rock fractions from deformed rocks from the Yushu mélange. Apparent age error bars are at the 1σ level; Errors in the J-parameter are not included. Plateau and pseudo-plateau ages (2σ uncertainties including errors in the J-parameter) are given when applicable. $^{39}Ar_K$ degassing spectra ($(^{39}Ar_K/DVT\circ)/(^{39}Ar_K/DVT\circ)Max$ vs. $\%^{39}Ar_K$) are provided for most of the experiments (See Tremblay et al. (2020) for a detailed explanation).

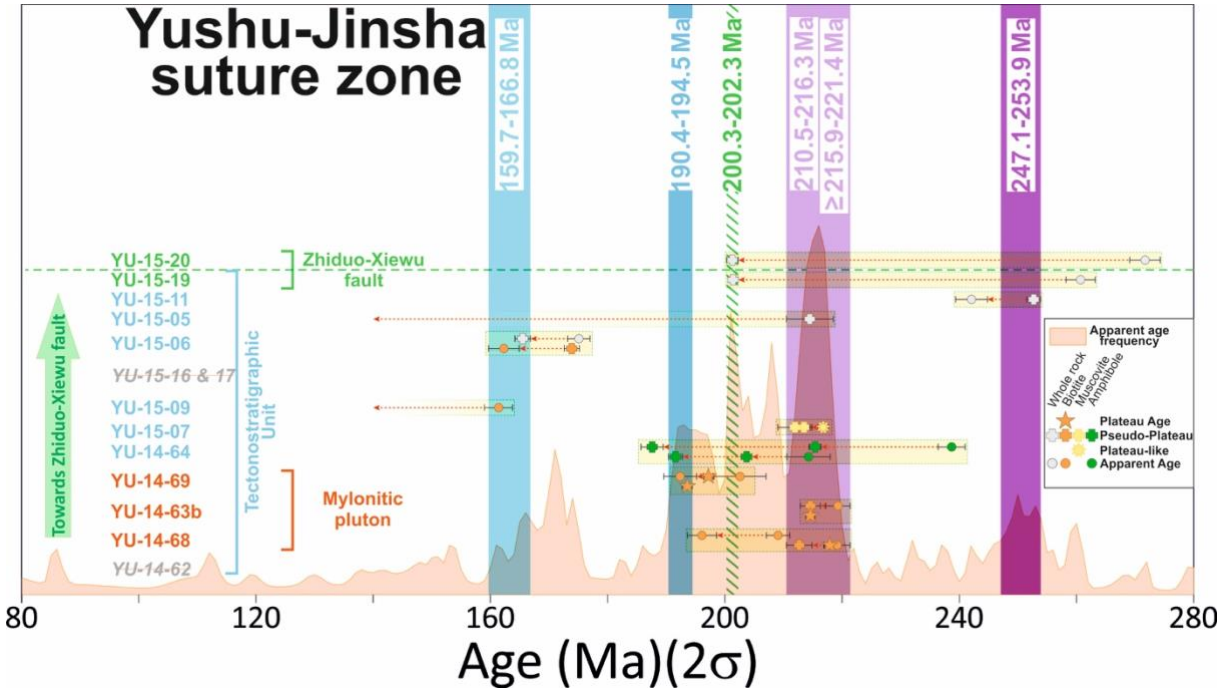

Figure 13. Synthesis of plateau, pseudo-plateau, plateau-like and apparent ages (2σ error bars) from $^{40}Ar/^{39}Ar$ analyses of whole rock (grey), biotite (brown), phengite (yellow) and amphibole (green) single grains from samples from the Tectonographic Unit and the Zhiduo-Xievu fault plotted against the frequency histogram (probability density diagrams) of the apparent ages (see Tremblay et al. (2020) for explanation). The samples are classified according to their sampling distance from the Zhiduo-Xiewu Fault. The main events identified by the $^{40}Ar/^{39}Ar$ geochronological study are highlighted by colour bars following the colour codes of the International Chronostratigraphic Chart. The significance of these periods is discussed in the text.

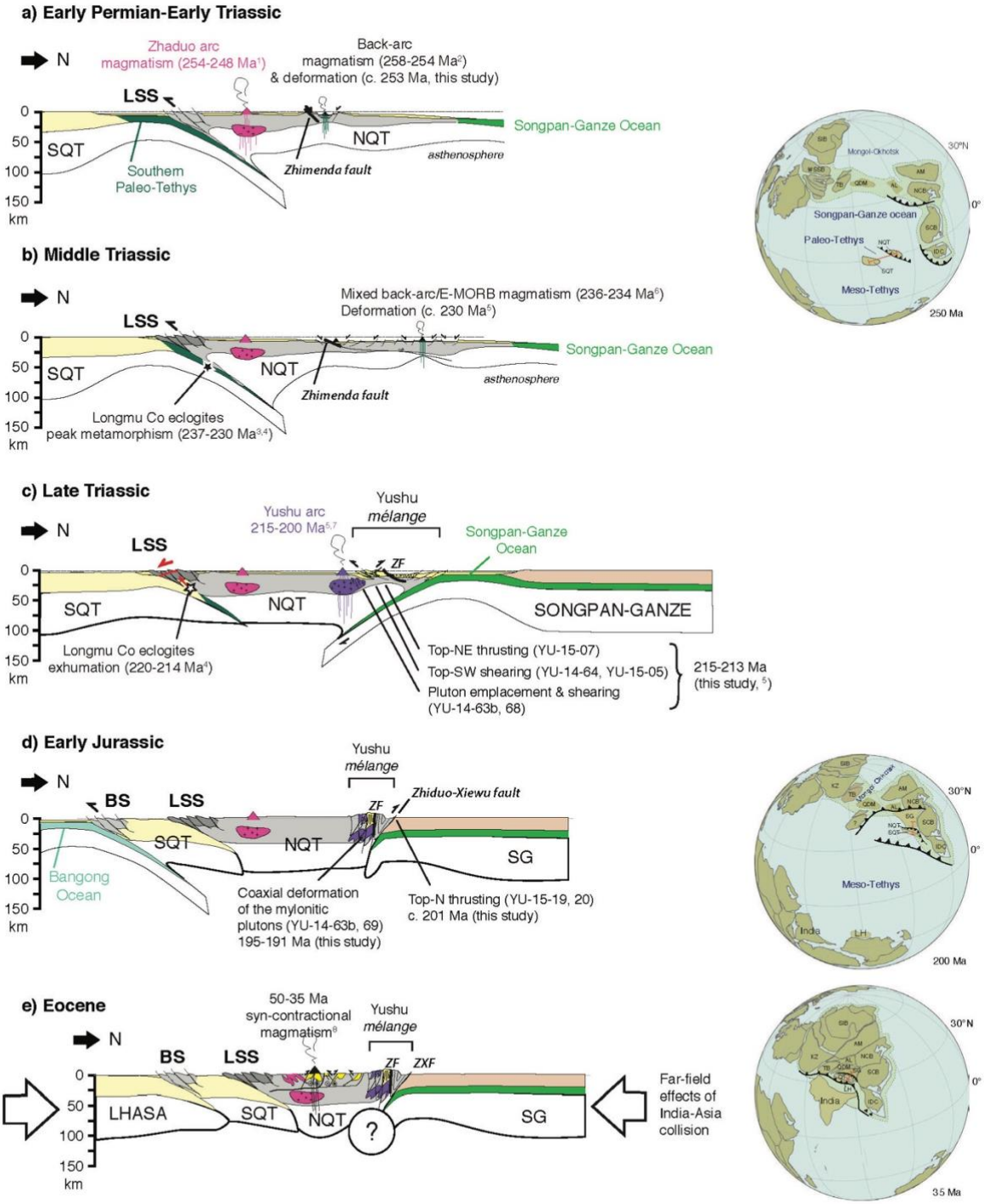

Figure 14. Schematic sketch (not to scale) of a possible geodynamic evolution of the Yushu area from the Permo-Triassic to the Eocene, reconciling the currently known ages of deformation and magmatism. Age data sources: [1]Yang et al. (2011); [2]Zhang et al. (2017); [3]Dan et al., 2018; [4]Zhai et al. (2011); [5]Yang et al. (2012); [6]Liu et al. (2016b); [7]Roger et al.

(2003); [8]Spurlin et al., 2005. Abbreviations: CQMB, Central Qiangtang Metamorphic Belt; BS, blueschist facies; JS, Jinsha-Ganze-Litang Suture; LSS, Longmu Co-Shuangu Suture; SQt, South Qiangtang; NQt, North Qiangtang.